Physical and chemical transformations of zirconium doped ceria nanoparticles in the presence of phosphate

Briffa, Sophie Marie; Lynch, Iseult; Hapiuk, Dimitri; Valsami-Jones, Eva

DOI:
10.1016/j.envpol.2019.06.014

Document Version
Publisher's PDF, also known as Version of record

Citation for published version (Harvard):
Briffa, SM, Lynch, I, Hapiuk, D & Valsami-Jones, E 2019, 'Physical and chemical transformations of zirconium doped ceria nanoparticles in the presence of phosphate: increasing realism in environmental fate and behaviour experiments', *Environmental Pollution*, vol. 252, no. Part B, pp. 974-981.
https://doi.org/10.1016/j.envpol.2019.06.014

Environmental Pollution 252 (2019) 974–981

Contents lists available at ScienceDirect

Environmental Pollution

journal homepage: www.elsevier.com/locate/envpol

Physical and chemical transformations of zirconium doped ceria nanoparticles in the presence of phosphate: Increasing realism in environmental fate and behaviour experiments☆

Sophie Marie Briffa [a, *], Iseult Lynch [a], Dimitri Hapiuk [b], Eugenia Valsami-Jones [a]

[a] School of Geography, Earth and Environmental Sciences, University of Birmingham, UK
[b] Nanoscale Physics Research Laboratory, School of Physics and Astronomy, University of Birmingham, UK

ARTICLE INFO

Article history:
Received 25 December 2018
Received in revised form
8 May 2019
Accepted 4 June 2019
Available online 7 June 2019

Keywords:
Cerium
Zirconium doped ceria
Cerium phosphate
Nanoparticles
Transformation
Environmental realism
Regulation

ABSTRACT

During their lifecycle, many engineered nanoparticles (ENPs) undergo significant transformations that may modify their toxicity, behaviour, and fate in the environment. Therefore, understanding the possible environmentally relevant transformations that ENPs may undergo as a result of their surroundings is becoming increasingly important. This work considers industrially produced ceria (CeO_2) and focuses on a particle library consisting of seven zirconium-doped variants ($Ce_{1-x}Zr_xO_2$) where the Zr doping range is $x = 0-1$. The study assesses their potential transformation in the presence of environmentally relevant concentrations of phosphate. These ENPs have an important role in the operation of automotive catalysts and therefore may end up in the environment where transformations can take place. Samples were exposed to pH adjusted (c. 5.5) solutions made up of either 1 mM or 5 mM each of KH_2PO_4, citric acid and ascorbic acid and the transformed particles were characterised by means of DLS – size and zeta potential, UV/VIS, TEM, FT-IR, EDX and XRD. Exposure to the phosphate solutions resulted in chemical and physical changes in all ceria-containing samples to cerium phosphate (with the monazite structure). The transformations were dependent on time, ceria concentration in the particles (Ce:Zr ratio) and phosphate to ceria ratio. The presence of Zr within the doped samples did not inhibit these transformations, yet the pure end member ZrO_2 ENPs showed no conversion to phosphate. The quite dramatic changes in size, structure and composition observed raise important questions regarding the relevant form of the materials to investigate in ecotoxicity tests, and for regulations based on one or more dimensions in the nanoscale.

1. Introduction

Once released into the environment, which can occur at any point during their lifecycle, ENPs undergo complex interactions with the abiotic and biotic constituents of their surroundings, leading to a range of competing possible transformations. These interactions and transformations are dependent on the intrinsic ENP properties and the environmental exposure scenario (extrinsic conditions). They vary from ENP to ENP as a function of their physicochemical properties, i.e. composition (Mitrano et al., 2015), size (Nowack and Bucheli, 2007; Rickerby and Morrison, 2007), shape/structure, surface area, charge, surface coating and chemical reactivity of the surface and solubility (Kim et al., 2010; Aydin et al., 2012; Thwala et al., 2013; Karakoti et al., 2012; Labille et al., 2010), and depend on the pH, alkalinity, salt and biomolecule composition of the receiving environment (Lynch et al., 2014a).

Transformations that ENPs undergo can be described as chemical (e.g. redox reactions), physical (e.g. agglomeration), and biological/biomolecular (Mitrano et al., 2015; Lowry et al., 2012; Louie et al., 2014). These transformations can determine the fate, behaviour and toxicity of ENPs (Mitrano et al., 2015; Lowry et al., 2012; Markiewicz et al., 2018; Lynch et al., 2014b). Therefore, understanding and determining these transformations could help to understand better the benefits or risks of these materials in different applications (Mitrano et al., 2015). Furthermore, it is important to understand and characterise the changes as they occur over time (Karakoti et al., 2012) as this is not yet well understood (Mudunkotuwa et al., 2012). Indeed, depending on how

☆ This paper has been recommended for acceptance by Baoshan Xing.
* Corresponding author.
E-mail address: BriffaSM@bham.ac.uk (S.M. Briffa).

https://doi.org/10.1016/j.envpol.2019.06.014

rapidly the transformations occur, there may be none of the original ENP present in the environment within a matter of minutes, raising important questions regarding which is the appropriate form to test for hazard and risk assessment, and indeed if the ENP transforms completely (e.g. dissolves to ionic species or transforms into larger sub-mircon or sub-millimeter particles) it may no longer fall under nano-specific testing guidelines.

This paper describes the physical and chemical changes induced on ceria (CeO_2) and zirconium doped ceria ($Ce_{1-x}Zr_xO_2$) ENPs on exposure to laboratory prepared phosphate solutions representative of likely environmental compositions of common soil pore waters. ENPs reaching soils, e.g. from road-surface run-off or as a result of air-borne deposition via rainfall for ceria ENPs utilised in catalytic conversters, may thus be exposed to phosphate-rich solutions, thus understanding their tranformations is essential to understand their environmental fate and ecotixicological hazard.

The uses of ceria are numerous, for example in optics, microelectronics, solid oxide fuel cells, solar cells, catalysis, bio-medical applications, oxidation resistance materials, UV absorbents and filters, antireflective coatings, abrasives for chemical mechanical planarization and metallurgical and glass/ceramic applications (Rajeshkumar and Naik, 2017; Briffa et al., 2017; Kuchibhatla et al., 2012). Zirconium doped ceria ENP systems are one of the most studied mixed-metal oxides in the literature due to their important role in the operation of automotive catalysts (Mudunkotuwa et al., 2012).

Literature has shown that rare earth oxides (REOs) interact with intracellular phosphates and transform at a low pH (Li et al., 2014), as a result of phosphate deposition on the particle surface following stripping of phosphate groups from the lysosomal membrane lipids (Li et al., 2014). However, unlike other REO ENPs studied, CeO_2 remained substantially nontransformed; the justification proposed by the authors for the lack of dissolution of CeO_2 is related to the lower solubility product, Ksp (10^{-53}) in water of tetravalent CeO_2 compared to the trivalent REOs (Ksp, 10^{-21}), coupled with the fact that the CeO_2 is highly insoluble at both pH 7 and 4.5 (Abreu and Morais, 2010). It is well known that CeO_2 ENPs are more soluble under acidic conditions and that Ce (III) ions have high binding affinity to phosphate groups, which can change their ultimate fate and toxicity (Li et al., 2014; Zhang et al., 2012; Rui et al., 2015; Singh et al., 2011). Thus, despite the lack of transformation under the specific conditions of the aforementioned study, phosphate-driven transformations are likely to happen in the environment, due to the ease with which CeO_2 reacts with phosphate (Singh et al., 2011) as well as the abundant natural presence of phosphorous and its compounds in the environment. Zhang et al. (2012) investigated the biochemical transformation of ceria ENPs in cucumber plants and observed that organic acids (e.g., citric acids) promoted CeO_2 dissolution while reducing substances (e.g., ascorbic acids) played a key role in the transformation process, generating Ce (III) ions which then reacted with the phosphate present in the medium. CeO_2 ENPs were transformed into needle-like $CePO_4$ clusers on the epidermis and in the intercellular spaces of cucumber roots, and to Ce-carboxylates in the shoots, despite the very low water solubility of CeO_2 in aquatic environments. CeO_2 ENP uptake was also observed in cilantro, but the CeO_2 ENPs were not transformed (Morales et al., 2013), suggesting that intermediates such as organic acids are required to first dissolve or reduce the Ce(IV) to Ce(III).

To systematically investigate the effect of phosphate on the transformation of CeO_2 ENPs, the effect of phosphate concentration, time and increasing amounts of Zr-doping of CeO_2 ENPs was assessed by exposing the range of $Ce_{1-x}Zr_xO_2$ ENPs to phosphate solutions (containing equimolar concetrations of citric and ascorbic acids) and carrying out physical and chemical characterisation of the ENPs at time 0, 7 days and 21 days. The ENPs were exposed to solutions of either 1 mM or 5 mM of monopotassium phosphate, with equimolar concentrations of reducing agents citric acid and ascorbic acid, whilst the pH of the solutions was adjusted to c. 5.5.

The phosphate concentrations were chosen to span the range of typical soil phosphate concentrations and thus allow assessment of the influence of phosphate concentration on the transformation. 1 mM phosphate is used in Hoagland hydroponic solutions widely used for plant growth experiments, while 5 mM results in an excess of phosphate such as could occur in areas prone to high agricultural run-off (Trejo-Téllez and Gómez-Merino, 2012). Ascorbic and citric acid are common organic acids found in soils and have been identified to play significant roles in soil productivity (Adeleke et al., 2017). Organic acids dissolved in soil pore water are on the order of 10^{-3} to 10^{-2} mmoldm^{-3} (Quideau and Bockheim, 1997). These act as the reducing agents required to induce CeO_2 ENP transformation, i.e. by reducing Ce(IV) to Ce(III), and are able to create a strong oxygen demand similar to that of flooded soils (e.g., wetlands) (Lowry et al., 2012; Lissner et al., 2003; Römer et al., 2019). The pH value was chosen based on previous studies by the authors (Römer et al., 2019), and the selected pH was the one where the largest degree of transformation of undoped CeO_2 ENPs took place, due to the fact that at this pH 100% of the available phosphorus is present as $H_2PO_4^-$. Finally, the optimum pH range for most plants is between 5.5 and 7.5.

2. Methodology

The ceria and zirconium doped ceria ENPs shown in Table 1 were used as received from Promethean Particles Ltd., Nottingham, UK (https://www.prometheanparticles.co.uk). STEM images for these particles are shown in Table S1 in the supporting information. All came as concentrated aqueous dispersions (~2.5 wt % particles). Monopotassium phosphate (Fisher Scientific), citric acid (Fisher Scientific) and ascorbic acid (Sigma-Aldrich) were also used as received from the supplier. Samples Ce-A – Ce-G (Table 1), which ranged from 100% CeO_2 to 100% ZrO_2 with varying Ce:Zr ratios in between, were exposed to laboratory prepared phosphate solutions based on the method of Zhang et al. (2012). Solutions containing 1 mM or 5 mM of each of monopotassium phosphate, citric acid and ascorbic acid were prepared and the pH of the phosphate solution was adjusted to c. 5.5. For each concentration (1 mM and 5 mM exposed) two series of samples were prepared (as some characterisation techniques required more concentrated samples).

- One where 1 mL of the ENP dispersion was added to 4 mL of the phosphate solution (resulting in concentrations ranging from 0.15 mM Ce: 4×10^{-3} mM (1 mM) or 0.02 mM (5 mM) P for sample Ce-A to 0 mM Ce: 4×10^{-3} mM (1 mM) or 0.02 mM (5 mM) P for sample Ce-G).
- One where 0.08 mL of the ENP dispersion was added to 4.92 mL of the phosphate solution (resulting in concentrations ranging

Table 1
Ceria and zirconium doped ceria ENPs (received from Promethean Particles Ltd.) used in this work. Their composition can be described by the formula: $Ce_{1-x}Zr_xO_2$, where x = 0–1.

Code	Chemical Formula
Ce-A	CeO_2
Ce-B	$Ce_{0.9}Zr_{0.1}O_2$
Ce-C	$Ce_{0.75}Zr_{0.25}O_2$
Ce-D	$Ce_{0.48}Zr_{0.52}O_2$
Ce-E	$Ce_{0.25}Zr_{0.75}O_2$
Ce-F	$Ce_{0.1}Zr_{0.9}O_2$
Ce-G	ZrO_2

from 1.16×10^{-2} mM Ce: 4.92×10^{-3} mM (1 mM) or 0.0246 mM (5 mM) P for sample Ce-A to 0 mM Ce: 4.92×10^{-3} mM (1 mM) or 0.0246 mM (5 mM) P for sample Ce-G).

Ageing was performed for 7 or 21 days at room temperature in the dark.

Samples were characterised as described below at time 0, day 7 and day 21 of exposed to the phosphate solutions.

Samples were characterised by means of dynamic light scattering (DLS), both for sizing and zeta potential, and UV/VIS spectroscopy before any exposure to phosphate (pristine ENPs), as well as immediately after phosphate solution addition, and at days 7 and 21 of exposure. For these analyses both the samples having a lower Ce:P ratio (i.e. the 0.08 mL samples) and higher Ce:P ratio (i.e. the 1 mL samples) were used. Pristine, 7 day old and 21 day old samples having a higher Ce:P ratio (i.e. the 1 mL samples) were further characterised by means of X-ray Diffraction (XRD), Fourier Transform Infrared Spectroscopy (FT-IR), Transmission Electron Microscopy (TEM) and Energy Dispersive X-ray Spectroscopy (EDX).

DLS measurements were performed on a Malvern Zetasizer (nano ZS) at 20 °C with samples equilibrated for 2 min before the measurements were started. Ten consecutive measurements of the "as prepared", time 0 (i.e. immediately upon addition of phosphate solution) and 7 and 21 day aged samples were collected and averaged to calculate the mean size. The same instrument was used to obtain the zeta potential of the "as prepared", time 0 and 7 and 21 day aged samples at 21 °C with samples equilibrated for 2 min before measurements were started. Three consecutive measurements were collected and averaged to calculate the zeta potential.

UV/VIS absorption readings were recorded in 10 cm quartz cuvettes for the more diluted samples (formed of 0.08 mL of the ENP dispersion) by means of a Jenway 6800 UV/vis spectrophotometer. A background spectrum was first obtained using ultrapure water followed by three sample readings, scanning from 800 to 220 nm. FT-IR spectra were obtained using a Varian 660-IR FT-IR Spectrophotometer on a few mg of sample which has been dried in a Gallenkamp hot box oven with a fan at 50 °C for 3 days. Prior to samples being analysed background scans were carried out.

TEM samples were prepared on copper grids coated with a thin film of holey carbon (Carbon film on 300 mesh Copper grids 3.05 mm) via the drop method using the higher Ce molar concentration samples (i.e. from the 1 mL ENP dispersions). This involves placing a drop of sample on the surface of the grid which was held stationary and suspended by means of TEM tweezers. The drop was allowed to stand on the grid for a period of half an hour to an hour to allow the ENPs to adhere to the surface of the grid. Following this the grids were gently dipped repeatedly in ultrapure water to remove any loose material and excess salts from the grid. Any

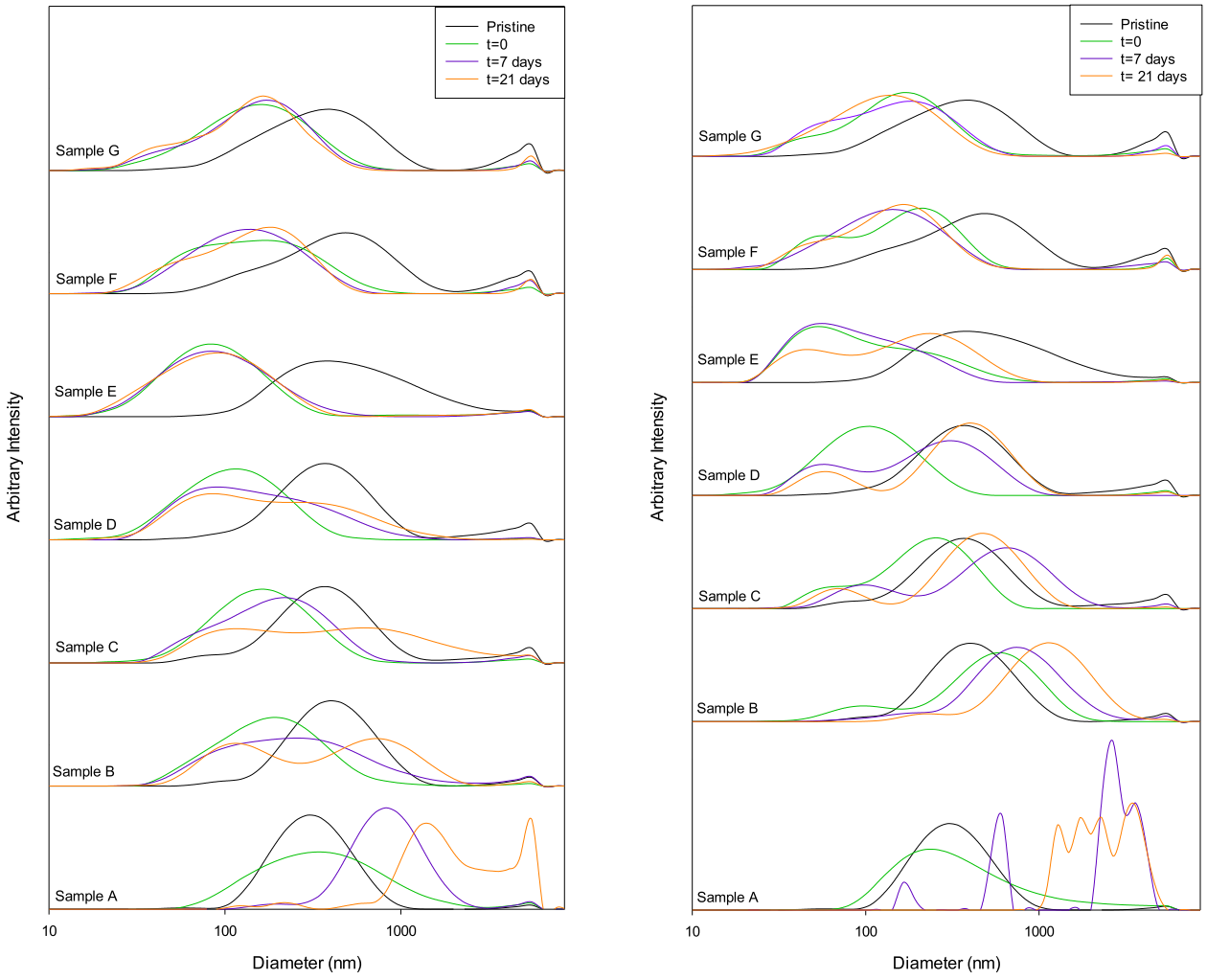

Fig. 1. DLS size histograms for the series of $Ce_{1-x}Zr_xO_2$ ENP samples A-G exposed to 1 mM (left) and 5 mM (right) phosphate solution (KH_2PO_4, citric acid and ascorbic acid) as a function of time.

excess water that remained was carefully removed with a tissue. The grids were allowed to air-dry and kept covered to prevent any contamination from taking place. Imaging was carried out using a JEOL 1200 TEM at an accelerating voltage of 80 kV, and a JEOL 2100 TEM (accelerating voltage 200 keV) and EDX spectroscopy was carried out using the JEOL 2100 TEM. Inca software was used to analyse the EDX spectra obtained.

3. Results and discussion

Phosphate ageing of the zirconium doped ceria ENPs resulted in both physical and chemical transformations for all ceria containing samples. Firstly, colour changes were noticed immediately upon addition of the 4 mL of phosphate solution, both 1 mM and 5 mM, to the ENPs. As the amount of ceria present within the Zr-doped CeO_2 ENP samples decreased, the colour changed from their initial purple-grey to white. Over time following the phosphate addition, the darker coloured samples became lighter in colour while the lighter coloured samples became darker. The final result was that the samples all looked yellow. No noticeable colour change was observed for the more dilute ENP samples.

DLS results (Fig. 1 (the raw data for which is shown in the supporting information (SI) S2 file)) revealed an immediate decrease in particle size upon phosphate addition. This is due to the change of the medium environment influencing the conductivity and electric double layer surrounding the ENPs. This initial decrease is followed by an increase in particle size, presumably as a result of the physical and chemical transformations taking place. The extent of the size increase is proportional to the Ce:Zr ratio within the sample (i.e. increasing from sample A to G). Phosphate concentration (Ce:P ratio) was found to influence the transformations also, as some changes, such as the increase in size between 7 and 21 days, were more noticeable for the 5 mM exposure compared to the 1 mM exposure.

The entire range of TEM images (obtained on the JEOL 1200) for all samples are shown in Table S2 in the SI, and representative examples are presented in Fig. 2. The images reveal the physical transformations that took place over time upon exposure of the ENPs to the phosphate solutions. Samples show transformation from spherical particles (Fig. 2a) to needle-shaped crystals growing outwards from a central point, that result in particles resembling sea-urchin structures as seen in Fig. 2b. Samples A to F all showed some form of this physical transformation. The degree of transformations decreased from sample A to sample G as the ceria concentration decreased, with sample G (100% ZrO_2) showing no transformation (Fig. 2c). Transformations thus decreased with the decrease in ceria content of the ENPs, from sea-urchins to needles to no transformation. Furthermore the degree of transformations observed varied between the samples exposed to the 1 mM and 5 mM phosphate solutions, with the greater concentration showing a greater extent of transformations. This evidences that phosphate concentration influenced the extent of transformation.

The sea-urchin formation appears to take place in a number of steps. Firstly the primary ENPs appear to decrease in size compared to the size of the pristine particles which is proably due to CeO_2 dissolution and reduction in the presence of citric and ascorbic acid, as observed from the UV/VIS results and discussed below. Once Ce (III) ions are generated they then react with the phosphate present

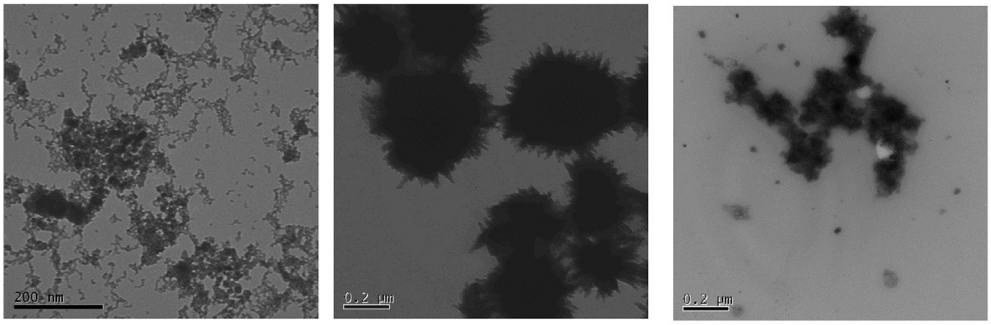

Fig. 2. TEM image of a) pristine CeO_2 (sample Ce-A) ENPs b) sample Ce-B showing sea-urchin shaped particles c) sample G showing no transformation. Images b and c were taken on samples aged for 21-days in 5 mM phosphate solution. The full set of particles, timepoints and phosphate concentrations are provided in the SI Fig. S1.

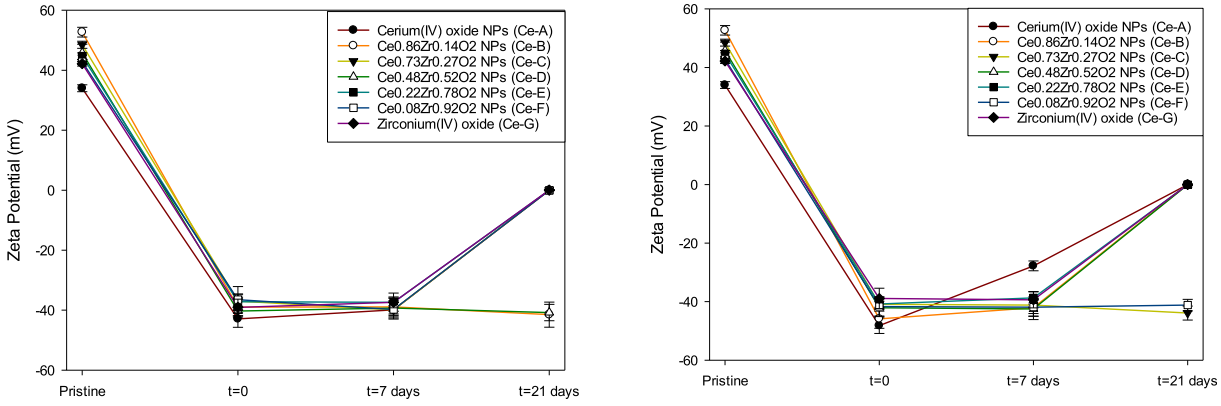

Fig. 3. Zeta Potential of $Ce_{1-x}Zr_xO_2$ ENP samples A-G exposed to 1 mM (left) and 5 mM (right) phosphate solution as a function of time.

in the medium. $CePO_4$ has a relatively low solubility in water (0.04 ± 0.04 millimolal), and as such reprecipitates rapidly (Tropper et al., 2013). This reprecipitation nucleates on the remaining surfaces of the original particles leading to formation of needles, which over time result in formation of larger sea-urchin like structures having a size of *circa* 200 nm. It is important to note that the resultant particles have different surface properties to the original particles which can affect reactivity and possible particle interactions within the environment or human body, which could in turn influence toxicity. The alterations in size and the needle-like structures can also play a role in bioavailability and uptake, which again impacts on toxicity.

Zeta potential results (Fig. 3 (the raw data for which is shown in the SI S3 file)) show that immediately upon addition of the phosphate solution the zeta potential values change from positive stable values of 34–53 mV to negative stable values of −36 to −43 mV for the 1 mM phosphate solution and to −38 to −49 mV for the 5 mM phosphate solution. In the presence of the new media containing KH_2PO_4, citric acid and ascorbic acid, a change in electrolyte concentration and pH (c. 5.5) occurs. Citric acid and ascorbic acid are electrostatically attracted to the initially positively charged ENP surfaces and bind, leading to highly negatively charged surfaces. The pH and ionic strength-driven association of the acidic groups from the citric acid and ascorbic acid on the surface of the ENPs further enhances the negatively charged surfaces. The phosphate ions then increase the surface charge density and change the charge of the ENP surface by displacing the acidic groups on the surface of the ENPs (Nelson et al., 2000). The fact that the highest Zr-containing ENPs remain highly negative confirms that there are no phosphate transformations as the surface of the ENPs stays negative meaning that the initially bound acidic groups remain on the surface.

Between t = 0 and t = 7 days limited changes are observed in all samples, whether exposed to 1 mM or 5 mM of phosphate, with the exception of the 100% CeO_2 ENP (Ce-A) exposed to 5 mM where the zeta potential value increases significantly towards 0. The phosphate ions begin to displace the absorbed acid groups increasing the surface charge of the ENPs. This is influenced by the exposure duration, the phosphate solution concentration and the Ce surface available. Hence, the zeta potential of sample Ce-A exposed to 5 mM increases most significantly.

By day 21, a more pronounced effect on the zeta potential values of the samples is observed, implying that time influences transformations and behaviour. The surface of the ENPs with the associated acid groups have more opportunity to be displaced by the phosphate groups at longer times.

In general, samples Ce-A, Ce-E and Ce-G follow the same trend regardless of the phosphate concentration. Samples Ce-B and Ce-D remain stable in the 1 mM solution but not the 5 mM solution implying that the increased concentration results in faster changes taking place. Samples Ce-C and Ce-F are unstable after 21 days in the 1 mM solution but stable in the 5 mM solution indicating that the relationship between the phosphate concentration and the ENP sample composition is a determining factor in the transformations.

FT-IR (Fig. 4 (the raw data for which is shown in SI S4 file)) shows the stretching peak for P-O at 960 cm^{-1} present in the spectrum of the exposed sample Ce-A. This indicates a chemical change from CeO_2 to cerium phosphate ($CePO_4$). The P-O peak is shadowed in samples Ce-B–Ce-G due to an –OH bending peak seen at 937 cm^{-1} for all zirconium containing samples. The weak peak seen for the aged samples at 1153 cm^{-1} can be attributed to P=O stretching. This peak is not observed for sample Ce-G (ZrO_2 ENP). In fact, no spectral differences are noted between the pristine and phosphate aged sample Ce-G, implying no chemical transformation took place for the ZrO_2 ENPs even after 21 days.

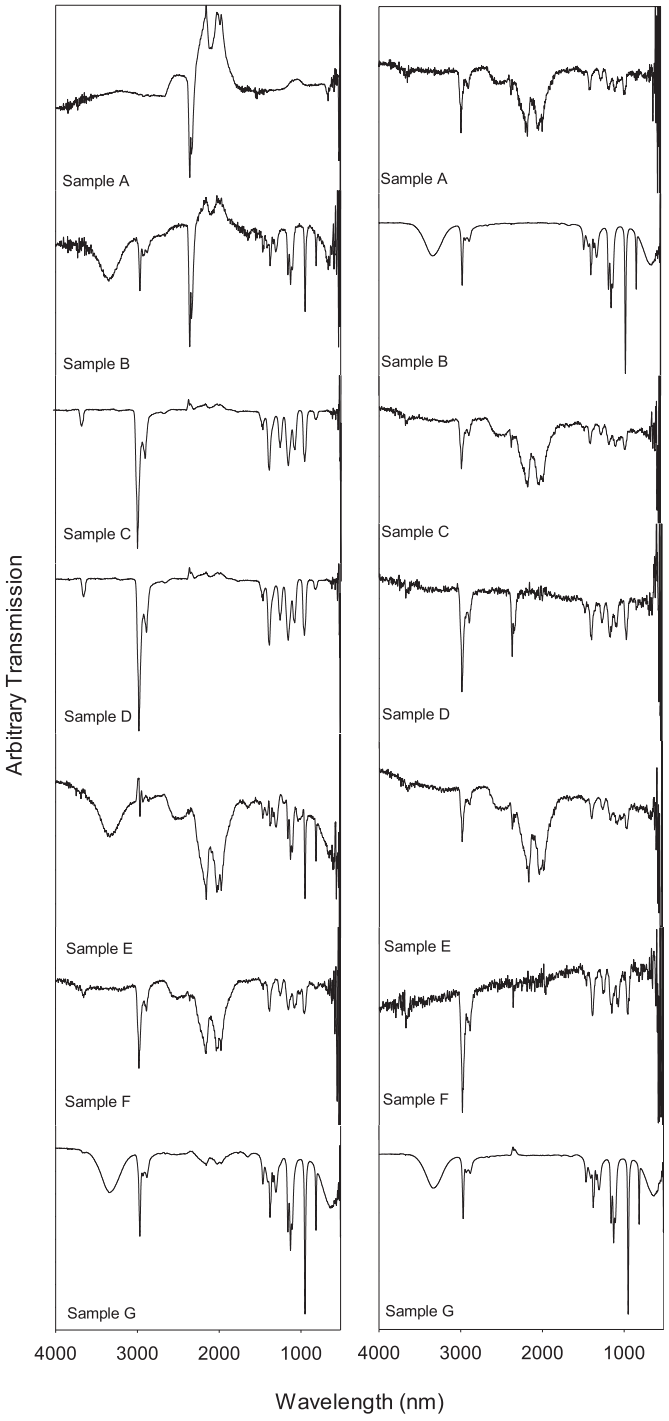

Fig. 4. FT-IR spectra for pristine (left) and 21 day 5 mM phosphate aged (right) samples A-G (top to bottom). The stretching peak for P-O at 960 cm^{-1} is present for Ce-A. The weak peak seen for the aged Ce-containing samples at 1153 cm^{-1} can be attributed to P=O stretching.

On analysing the UV-VIS spectra (Fig. S1 in the SI (the raw data for which is shown in SI S6 file)) the pristine spectra, sample Ce-A clearly shows the cerium (IV) absorbance peak between 300 and 400 nm. This is due to the charge-transfer transition between O *2p* and Ce *4f* bands (Herrling et al., 2013; Tsunekawa et al., 2000). The intensity of this peak decreases to non-existent across samples Ce-B–Ce-G as the cerium concentration decreases to 0 in sample Ce-G, the pure ZrO_2 ENP. The pristine Ce-G spectrum shows a peak at c.

240 nm which literature has attributed to both tetragonal and monoclinic ZrO_2 (Ranga Rao and Sahu, 2001) and a peak near 290 nm which can be attributed to interstitial Zr^{3+} ions in the monoclinic lattice (Kumari et al., 2009).

On addition of the phosphate solution a strong peak can be seen immediately at c. 270 nm, which is most likely due to presence of ascorbic acid adsorption at the ENP surfaces, and could well be overshadowing the Ce (III) peak. Between day 7 and day 21, only differences in peak intensity were noticed with no significant peak position changes recorded, indicating that no new transformations were occurring, but rather that the initial transformations were continuing to intensify (i.e. the amount of $CePO_4$ deposition as needle-like structure increased in samples Ce-A to Ce-F).

The XRD spectrum (Fig. 5 (the raw data for which is shown in SI S5 file)) for pristine CeO_2 ENPs (Ce-A) shows peaks (indicated with green stars) at $2\theta = 28$, 47 and 56 ° representing miller indices (111), (220) and (311) respectively (Lawrence et al., 2011). ZrO_2 ENPs (Ce-G) at the other end of the sample spectrum was identified as having a monoclinic structure, which is the structure adopted by ZrO_2 at room temperature. Peaks (indicated with black stars) are observed at $2\theta = 28.2$, 33.8, 35.1, 50.3 and 57.7 °, representing miller indices (111), (002), (200), (122) and ($2\bar{2}2$) respectively (Joint committee on powder, 2001). Pristine samples Ce-B–Ce-F showed both CeO_2 and ZrO_2 influenced lattice peaks since they are composed of $Ce_{1-x}Zr_xO_2$. As the series progresses from Ce-B to Ce-F as expected similarities pertaining to CeO_2 decrease and those pertaining to ZrO_2 increase, as shown in Fig. 5.

XRD revealed and confirmed the chemical transformations undergone by the $Ce_{1-x}Zr_xO_2$ ENP series following exposure to the phosphate solutions. After 21 days an increase in crystallinity could be noted at both phosphate concentrations. All cerium containing samples (Ce-A–Ce-F) show peaks attributed to cerium phosphate ($CePO_4$). The $CePO_4$ monazite peaks (indicated with blue stars) are most clearly seen in sample A. These are found at $2\theta = 25$, 27, 28, 41 and 48.5 ° representing miller indices (020), (200), (120), (013) and (103) respectively. The $CePO_4$ peaks become less obvious as the series progresses from sample Ce-A to Ce-F as a result of the reduced Ce available for dissolution and re-precipitation as $CePO_4$. Sample G shows peaks belonging to the starting reaction reagent potassium phosphate (indicated with red stars), and ZrO_2. No transformation was observed for the ZrO_2 ENPs, confirming that the ceria is the material undergoing transformation. Most notably, these results indicate that the ZrO_2 does not inhibit the transformation of the ceria within the doped samples.

The EDX results (Table 2) show sample Ce-A to contain potassium, cerium, phosphorous and oxygen and, as expected, to lack zirconium. Samples Ce-B–Ce-F show the presence of all the same components as Ce-A along with zirconium. Furthermore, the needles and core of the sea-urchin structures do not differ in compositional components, which suggests that the $CePO_4$ is diffusing into the core of the particles also before precipitating. The spectrum for Ce-G shows no cerium but identifies potassium, zirconium,

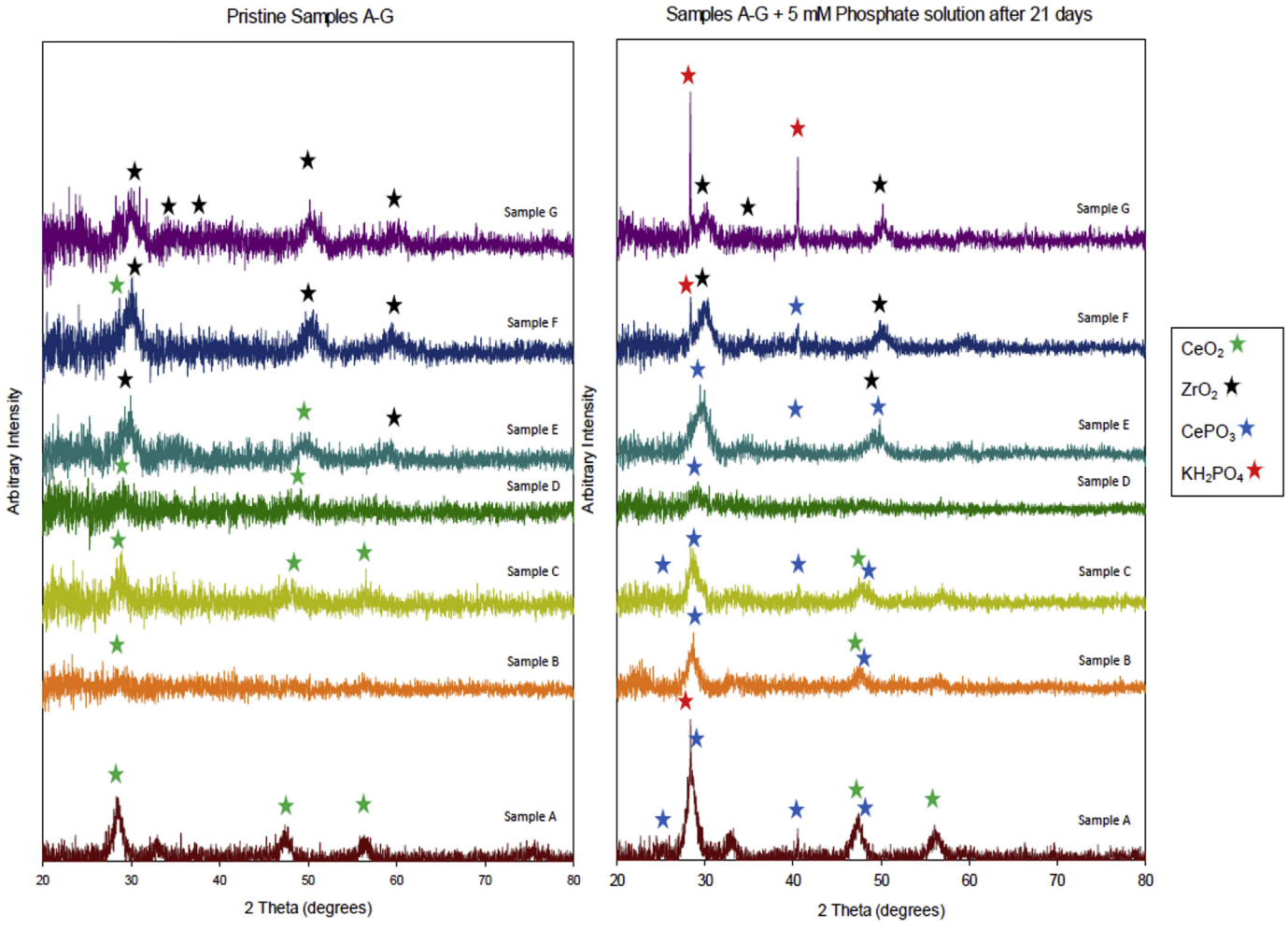

Fig. 5. XRD patterns for the pristine (left) and 21 day 5 mM phosphate aged (right) samples Ce-A-Ce-G (bottom to top).

Table 2
TEM images and EDX spectra for samples Ce-B, Ce-C and Ce-G exposed to 5 mM phosphate solution for 21 days. The remaining samples are provided in the SI Table S3.

Sample	Image	EDX Spectrum
Sample B	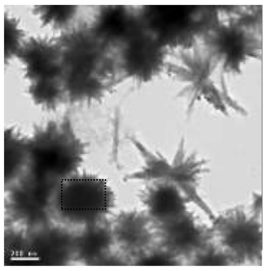	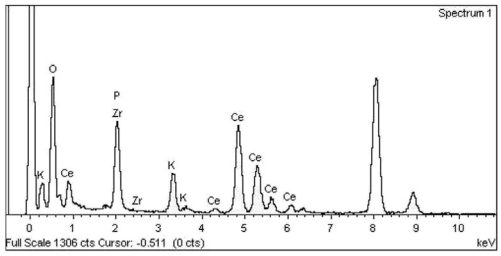
Sample C	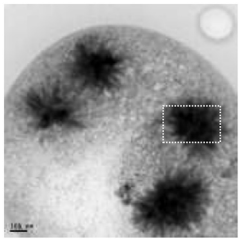	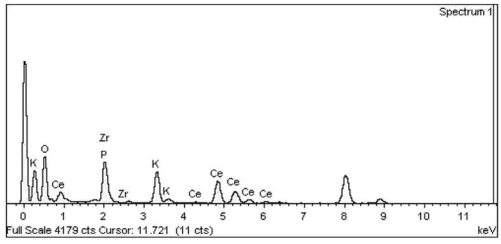
Sample G	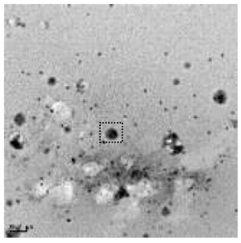	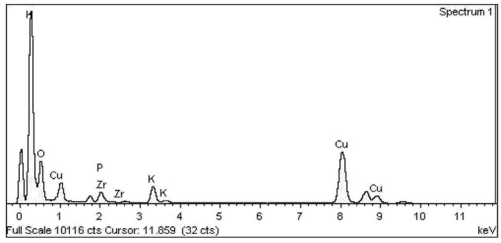

phosphorous and oxygen. The potassium and phosphorous are due to the initial reaction reagent, namely potassium phosphate, and are in the background rather than being ENP-associated.

4. Conclusion

This work studied the environmentally relevant phosphate induced transformations of zirconium-doped cerium dioxide ENPs, such as those used extensively in automotive catalysts, and the factors influencing the degree of transformation. To date, these transformations had only been observed for pure CeO_2 ENPs and not for doped CeO_2 ENPs, highlighting that the presence of doping does not inhibit transformations.

In the study, a series of zirconium-doped cerium dioxide ($Ce_{1-x}Zr_xO_2$) ENPs with varying Ce:Zr ratios (Zr-doping amounts from 0 to 100%) were exposed to environmentally realistic phosphate solutions (i.e. relevant pH, ionic strength, and small reducing molecules such as citric acid and ascorbic acid), resulting in physical and chemical transformations for all ceria-containing ENPs. Ceria and ceria-rich samples underwent transformation to larger particles growing into characteristic “sea urchin”/needle-like of chemical composition $CePO_4$/$Ce_{1-x}Zr_xPO_4$. Furthermore these samples underwent compositional transformation to phosphate-bearing phases. The transformations were dependent on time, ceria concentration, and phosphate to ceria ratio. The degree to which the transformation takes place varied depending on the Ce:Zr ratio and the phosphate solution concentration. The ZrO_2 ENPs showed no transformation to phosphate. However, the presence of zirconium within the doped samples did not inhibit these transformations for the Ce-containing ENPs.

The transformations observed in this work could occur in nature under ordinary environmental conditions, when ceria and ceria-containing ENPs find their way into phosphate-bearing media such as soil pore water at some stage during their lifecycle. These transformations can occur to different extents as seen depending on the conditions. Such changes in physical and chemical properties can easily induce transformations to materials with a new range of physicochemical properties that in turn influence the behaviour and possibly the toxicity of the ENPs. The present study highlights the importance of understanding the transformations undergone by ENP in the environment, in order to make informed decisions as to the particle form to test for ecotoxicity as part of risk assessment and regulation. It is clear that the rapid transformations of the $Ce_{1-x}Zr_xO_2$ ENPs to >200 nm sea-urchin $Ce_{1-x}Zr_xPO_4$ particles will have dramatic consequnces for their bioavailability and uptake by organisms, likely reducing their toxicity, but the needle-like structures may lead to physical damage such as membrane puncture, or may induce inflammatory processes such as frustrated phagocytosis if the particles are too large to be engulfed by macrophages for example.

Acknowledgments

The authors acknowledge partial financial support from EU FP7 funded project NanoMILE (Grant Agreement no 310451) and the Endeavour Scholarship Scheme (Group B). The authors would also like to acknowledge Theresa Morris from the School of Metallurgy and Materials at the University of Birmingham for help with EDX.

Appendix A. Supplementary data

Supplementary data to this article can be found online at https://doi.org/10.1016/j.envpol.2019.06.014.

References

Abreu, R.D., Morais, C.A., 2010. Purification of rare earth elements from monazite sulphuric acid leach liquor and the production of high-purity ceric oxide. Miner. Eng. 23 (6), 536–540.

Adeleke, R., Nwangburuka, C., Oboirien, B., 2017. Origins, roles and fate of organic acids in soils: a review. South Afr. J. Bot. 108, 393–406.

Aydin, A., Sipahi, H., Charehsaz, M., 2012. Nanoparticles toxicity and their routes of exposures. In: Recent Advances in Novel Drug Carrier Systems.

Briffa, S.M., et al., 2017. Development of scalable and versatile nanomaterial libraries for nanosafety studies: polyvinylpyrrolidone (PVP) capped metal oxide nanoparticles. RSC Adv. 7 (7), 3894–3906.

Herrling, T., Seifert, M., Jung, K., 2013. Cerium dioxide: future UV-filter in sunscreen? SOWF 139 (5), 10–15.

Joint committee on powder diffraction standards, Diffraction Data File no. 37-1484. In: International Centre for Diffraction Data, 2001.

Karakoti, A.S., et al., 2012. Preparation and characterization challenges to understanding environmental and biological impacts of ceria nanoparticles. Surf. Interface Anal. 44 (8), 882–889.

Kim, K.T., et al., 2010. Oxidative stress responses of Daphnia magna exposed to TiO2 nanoparticles according to size fraction. Sci. Total Environ. 408 (10), 2268–2272.

Kuchibhatla, S.V.N.T., et al., 2012. Influence of aging and environment on nanoparticle chemistry: implication to confinement effects in Nanoceria. J. Phys. Chem. C 116 (26), 14108–14114.

Kumari, L., et al., 2009. Controlled hydrothermal synthesis of zirconium oxide nanostructures and their optical properties. Cryst. Growth Des. 9 (9), 3874–3880.

Labille, J., et al., 2010. Aging of TiO2 nanocomposites used in sunscreen. Dispersion and fate of the degradation products in aqueous environment. Environ. Pollut. 158 (12), 3482–3489.

Lawrence, N.J., Jiang, K., Cheung, C.L., 2011. Formation of a porous cerium oxide membrane by anodization. Chem. Commun. 47 (9), 2703–2705.

Li, R., et al., 2014. Surface interactions with compartmentalized cellular phosphates explain rare earth oxide nanoparticle hazard and provide opportunities for safer design. ACS Nano 8 (2), 1771–1783.

Lissner, J., Mendelssohn, I.A., Anastasiou, C.J., 2003. A method for cultivating plants under controlled redox intensities in hydroponics. Aquat. Bot. 76 (2), 93–108.

Louie, S.M., Ma, R., Lowry, G.V., 2014. Chapter 2 - transformations of nanomaterials in the environment. In: Jamie, R.L., Eugenia, V.-J. (Eds.), Frontiers of Nanoscience. Elsevier, pp. 55–87.

Lowry, G.V., et al., 2012. Transformations of nanomaterials in the environment. Environ. Sci. Technol. 46 (13), 6893–6899.

Lynch, I., et al., 2014. Chapter 4 - macromolecular coronas and their importance in nanotoxicology and nanoecotoxicology. In: Lead, J.R., Valsami-Jones, E. (Eds.), Frontiers of Nanoscience. Elsevier, pp. 127–156.

Lynch, I., et al., 2014. Chapter 4 - macromolecular coronas and their importance in nanotoxicology and nanoecotoxicology. In: Jamie, R.L., Eugenia, V.-J. (Eds.), Frontiers of Nanoscience. Elsevier, pp. 127–156.

Markiewicz, M., et al., 2018. Changing environments and biomolecule coronas: consequences and challenges for the design of environmentally acceptable engineered nanoparticles. Green Chem. 20 (18), 4133–4168.

Mitrano, D.M., et al., 2015. Review of nanomaterial aging and transformations through the life cycle of nano-enhanced products. Environ. Int. 77, 132–147.

Morales, M.I., et al., 2013. Toxicity assessment of cerium oxide nanoparticles in cilantro (coriandrum sativum L.) plants grown in organic soil. J. Agric. Food Chem. 61 (26), 6224–6230.

Mudunkotuwa, I.A., Pettibone, J.M., Grassian, V.H., 2012. Environmental implications of nanoparticle aging in the processing and fate of copper-based nanomaterials. Environ. Sci. Technol. 46 (13), 7001–7010.

Nelson, B.P., et al., 2000. Control of surface and ζ potentials on nanoporous TiO 2 films by potential-determining and specifically adsorbed ions. Langmuir 16 (15), 6094–6101.

Nowack, B., Bucheli, T.D., 2007. Occurrence, behavior and effects of nanoparticles in the environment. Environ. Pollut. 150 (1), 5–22.

Quideau, S.A., Bockheim, J.G., 1997. Biogeochemical cycling following planting to red pine on a Sandy prairie soil. J. Environ. Qual. 26 (4), 1167–1175.

Rajeshkumar, S., Naik, P., 2017. Synthesis and biomedical applications of Cerium oxide nanoparticles - a Review. Biotechnology reports (Amsterdam, Netherlands) 17, 1–5.

Ranga Rao, G., Sahu, H.R., 2001. XRD and UV-Vis diffuse reflectance analysis of CeO2-ZrO2 solid solutions synthesized by combustion method. J. Chem. Sci. 113 (5), 651–658.

Rickerby, D.G., Morrison, M., 2007. Nanotechnology and the environment: a European perspective. Sci. Technol. Adv. Mater. 8 (1–2), 19–24.

Römer, I., et al., 2019. Impact of Particle Size, Oxidation State and Capping Agent of Different Cerium Dioxide Nanoparticles on the Phosphate-Induced Transformations at Different pH and Concentration. PloS One 14 (6), e0217483. https://doi.org/10.1371/journal.pone.0217483.

Rui, Y., et al., 2015. Transformation of ceria nanoparticles in cucumber plants is influenced by phosphate. Environ. Pollut. 198, 8–14.

Singh, S., et al., 2011. A phosphate-dependent shift in redox state of cerium oxide nanoparticles and its effects on catalytic properties. Biomaterials 32 (28), 6745–6753.

Thwala, M., et al., 2013. The oxidative toxicity of Ag and ZnO nanoparticles towards the aquatic plant Spirodela punctuta and the role of testing media parameters. Environmental Science-Processes & Impacts 15 (10), 1830–1843.

Trejo-Téllez, L.I., Gómez-Merino, F.C., 2012. Nutrient solutions for hydroponic systems. In: Hydroponics-a Standard Methodology for Plant Biological Researches (IntechOpen).

Tropper, P., Manning, C.E., Harlov, D.E., 2013. Experimental determination of CePO4 and YPO4 solubilities in H2O–NaF at 800°C and 1 GPa: implications for rare earth element transport in high-grade metamorphic fluids. Geofluids 13 (3), 372–380.

Tsunekawa, S., Fukuda, T., Kasuya, A., 2000. Blue shift in ultraviolet absorption spectra of monodisperse CeO2−x nanoparticles. J. Appl. Phys. 87 (3), 1318–1321.

Zhang, P., et al., 2012. Biotransformation of ceria nanoparticles in cucumber plants. ACS Nano 6 (11), 9943–9950.